

Numerical Investigation of Cavitation Interacting with Pressure Wave

J. G. Zheng^{1,2} and B. C. Khoo^{1,2,3,*}

¹ Temasek Laboratories, National University of Singapore, Singapore 117411.

² Department of Mechanical Engineering, National University of Singapore, Singapore 119260.

³ Singapore-MIT Alliance, National University of Singapore, Singapore 117576.

Received 17 April 2013; Accepted 3 March 2014

Available online 11 November 2014

Abstract. A computational fluid dynamics solver based on homogeneous cavitation model is employed to compute the two-phase cavitating flow. The model treats the two-phase regime as the homogeneous mixture of liquid and vapour which are locally assumed to be under both kinetic and thermodynamic equilibrium. As our focus is on pressure wave formation, propagation and its impact on cavitation bubble, the compressibility effects of liquid water have to be accounted for and hence the flow is considered to be compressible. The cavitating flow disturbed by the introduced pressure wave is simulated to investigate the unsteady features of cavitation due to the external perturbations. It is observed that the cavity becomes unstable, locally experiencing deformation or collapse, which depends on the shock wave intensity and freestream flow speed.

AMS subject classifications: 35L40, 65M08, 65M22, 76T10

Key words: Isentropic cavitation model, cavitating flow, pressure wave.

1. Introduction

Cavitation is fairly widespread in numerous engineering applications and is an undesired phenomenon in most situations. For operating underwater devices, the cavitation bubble collapse is usually accompanied by huge pressure surge, which will cause material erosion, noise, vibration, loss of efficiency, etc. Therefore, the prevention of cavitation occurrence has been the subject of a large body of research for the past many decades. However, the cavitation may also be beneficial to reduction of drag on underwater weapons such as that found for supercavitating torpedo.

*Corresponding author. *Email addresses:* ts1zhen@nus.edu.sg (J. G. Zheng), mpekbc@nus.edu.sg (B. C. Khoo)

A number of numerical difficulties are encountered in the modeling of cavitation and can be attributed to several reasons. First, the liquid flow is usually in low Mach number (Ma) regime. To speed up the convergence of numerical solution, some acceleration techniques like preconditioning have to be adopted. Second, there are large discontinuities in fluid properties including the density and Mach number across the cavitation boundary. This may lead to numerical instability and spurious pressure oscillations. In addition, a variety of complex physical procedures occur on the interfacial region such as phase transition, heat and mass transfer, etc. and modeling these physics is not easy. One class of cavitation models that gain wide use is built by including source terms in the governing equations to account for the finite rate phase transition between liquid and vapour [5, 7, 8, 13, 14, 19]. This kind of methods is physically reasonable but may not be accurate as expected because many parameters involved the models have to be determined empirically. Another popular class of models is based on the assumption that the phase transition occurs instantaneously [4, 6, 9–11]. The appropriate equation of states (EOS) are used to close the models. This type of methods appears simpler. However, the stiffness of EOS may pose severe numerical difficulties in simulation.

The majority of existing cavitation models ignore the liquid compressibility and are built based on the incompressible Navier-Stokes equations. This is consistent with experimental observation that the density of liquid element almost does not vary as long as there is no phase change and the flow velocity is not very high. This treatment is proved to be valid for a wide range of steady state problems [10, 11]. However, in this study, we are concerned with the unsteady dynamics of cavitation impacted by the pressure wave. Hence, the wave propagation and compressibility effects of liquid must be taken into account. The prediction and understanding of pressure wave propagation and its interaction with cavitation bubble and the resulting unsteady flow features are of great importance to stability of cavitation and the possible prevention of its collapse. Unfortunately, few works on this topic are found in the literature except for say [20]. This is the motivation of the present study. Here, the cavitating flow is governed by one-fluid homogeneous cavitation model which is based on the compressible Euler equations. The thermodynamic behaviors of pure liquid and liquid-vapour mixture in cavitation region are described by Tait EOS and isentropic cavitation model, respectively. The governing equations are discretized using a second-order accurate finite volume method. The cavitating flow driven by the introduced pressure wave is resolved and the unsteady features of supercavitation are investigated and analyzed.

The paper is organized as follows. In Section 2, the physical model and numerical method are described. In Section 3, the numerical results are presented and discussed. The conclusion is given in Section 4.

2. Physical model and numerical method

2.1. Governing equations

To model wave dynamics and wave-cavitation interaction, the cavitating flow must be assumed to be compressible and thus the time-dependent Euler equations are em-

ployed and given by,

$$\frac{\partial U}{\partial t} + \frac{\partial F}{\partial x} + \frac{\partial G}{\partial y} = -(i-1)H, \quad (2.1)$$

where i takes on the value of 1 and 2 for planar and axisymmetric flows, respectively. Here, U , F , G and H are the vector of conserved variables, inviscid flux vectors in x and y directions, axisymmetric source terms, respectively, and given by,

$$U = \begin{pmatrix} \rho \\ \rho u \\ \rho v \end{pmatrix}, \quad F = \begin{pmatrix} \rho u \\ \rho u^2 + p \\ \rho uv \end{pmatrix}, \quad G = \begin{pmatrix} \rho v \\ \rho uv \\ \rho v^2 + p \end{pmatrix}, \quad H = \frac{1}{y} \begin{pmatrix} \rho v \\ \rho uv \\ \rho v^2 \end{pmatrix}. \quad (2.2)$$

In (2.2), ρ is the density, u is the x velocity component, v is the y velocity component and p is the pressure. The set of partial differential equations (2.1) is able to model both the pure liquid flow and liquid-vapour mixture.

To close system (2.1), equation of state needs to be constructed. For liquid phase, an established EOS is the Tait EOS and given by,

$$p = B \left(\frac{\rho}{\rho_0} \right)^N - B + A, \quad p \geq p_{sat}, \quad (2.3)$$

where ρ_0 , A , B and N are material-dependent constants and take values of 1000 kg/m^3 , $A = 10^5 \text{ Pa}$, $B = 3.31 \times 10^9 \text{ Pa}$ and 7.15, respectively for water. Here, p_{sat} is the saturated vapour pressure.

When the pressure locally drops below the saturation pressure p_{sat} , liquid is vaporized and cavitation results. The resulting cavitating flow is described as the homogeneous mixture of liquid and vapour phases which are assumed to be under both kinetic and thermodynamic equilibrium. In a fluid element, the liquid and vapour share the same velocity, pressure and temperature, and the mixture density in (2.1) is defined as the convex combination of saturated liquid and vapour densities,

$$\rho = \alpha \rho_{sv} + (1 - \alpha) \rho_{sw} \quad (2.4)$$

with α being the volume fraction of vapour or void fraction. The two-phase mixture is modeled by the isentropic cavitation model [6],

$$\rho = \frac{k \rho_v^{cav} + \rho_l^{cav}}{\left(\frac{p+B-A}{p_{cav}+B-A} \right)^{-1/N} + k \left(\frac{p}{p_{cav}} \right)^{-1/\gamma}}, \quad p < p_{sat}, \quad (2.5)$$

where $k = \alpha_0 / (1 - \alpha_0)$ and α_0 is the known void fraction of the mixture density at p_{sat} . Here, ρ_v^{cav} and ρ_l^{cav} are the associated vapour and liquid densities at the cavitation pressure p_{cav} . The sound speed of the mixture can be derived theoretically and given by [18],

$$a = \left\{ \rho \left[\frac{\alpha}{\rho_{sv} a_v^2} + \frac{1 - \alpha}{\rho_{sw} a_w^2} \right] \right\}^{-\frac{1}{2}}, \quad (2.6)$$

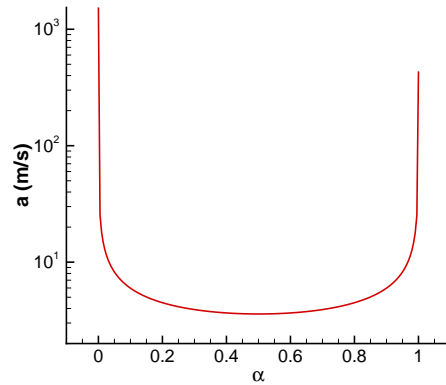


Figure 1: Speed of sound versus void fraction.

where a_v and a_w are the speeds of sound of vapour and liquid at the saturated pressure, respectively. It is found that the sound speed strongly depends on the void fraction α as illustrated in Fig. 1.

In model (2.1), the viscous effects are neglected as experimental observations indicate that cavitating flow is only weakly dependent on the Reynolds number and thus this approximation is reasonable [10, 11]. Of course, the inclusion of viscous effects in the model is also possible and easy to implement.

2.2. Numerical algorithm

In this subsection, the main numerical algorithms of our computational fluid dynamics (CFD) code are described briefly and more details on the numerics can be found in [20]. Using the method of lines, the spatial and temporal derivatives can be discretized separately. This approach offers us a lot of flexibility to select the appropriate numerical schemes for the spatial and temporal discretizations, separately.

The system of compressible Euler equations (2.1) is discretized using a finite volume method with a standard cell-based discretization technique. The computational mesh is generated by dividing the physical domain into a set of triangular elements. The control volumes on which the model (2.1) is integrated are the triangular elements themselves. A schematic cell is illustrated in Fig. 2. For the cell-centered scheme, the flow variables are associated with the cell centroids. The semi-discrete integral form of system (2.1) on control volume p in Fig. 2 is given by,

$$\int_{\Omega_p} \frac{\partial U}{\partial t} d\Omega = \sum_{k \in N(p)} (\tilde{F}_{pk} n_{k,x} + \tilde{G}_{pk} n_{k,y}) \Delta S + \tilde{H}_p \Omega_p = \int_{\Omega_p} \frac{\partial U}{\partial t} d\Omega + R_p(U) = 0, \quad (2.7)$$

where \tilde{F}_{pk} , \tilde{G}_{pk} and \tilde{H}_p are the numerical approximation of convective fluxes on edge $k = q, r, s$ and source terms, respectively. $R_p(U)$ is the residual. $N(p)$ represents the list of edges of cell p , ΔS_{pk} is the length of edge k and Ω_p is the area of cell p .

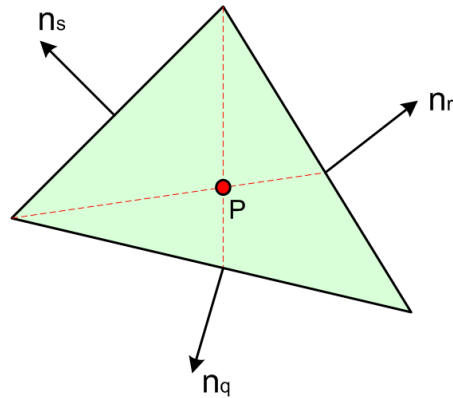


Figure 2: A grid cell and unit outward vector normal to cell face.

In our code, the numerical flux corresponding to the convective terms at edge midpoint is calculated by solving a Riemann problem using the classical Harten-Lax-van Leer (HLL) approximate Riemann solver [15] with the input state reconstructed separately on both sides of midpoint from the flow variables at centroids of two cells sharing the common edge. The second-order spatial accuracy is achieved by using the monotone upstream-centered schemes for conservation laws (MUSCL) [16, 17] with an appropriate limiter. However, one has to know the gradients of primitive variables including the density and velocity components at each centroid. Here, the gradients are determined based on Green-Gauss method and limited by Barth's limiter to prevent the generation of spurious oscillations across sharp gradients such as shock wave [1].

The time-marching is handled using the two-stage Runge-Kutta method [12],

$$U^{(1)} = U^{(n)} - \Delta t R(U^{(n)}), \quad (2.8a)$$

$$U^{(n+1)} = \frac{1}{2}(U^{(n)} + U^{(1)}) - \frac{1}{2\Delta t} R(U^{(1)}), \quad (2.8b)$$

with Δt being time step constrained by Courant-Friedrichs-Lewy (CFL) condition.

It is found that the treatment of boundary conditions, especially solid wall, is crucial to ensure the stability of our method. In this study, we use ghost cells which are virtual layers of cells outside the computational domain to implement various boundary conditions. The values of primitive variables in the ghost cells are obtained based on boundary type. The detailed discussion of boundary condition is found in [20].

It may be noted that our assembled code has undergone a series of preliminary tests with comparison to analysis and experimental results [20]. Although our method proves to be stable, robust, accurate, time-efficient and oscillation-free, we remain committed to any published experimental results on cavitating flow dynamics so as to further compare our numerical calculations.

3. Numerical results

3.1. Accuracy check

Due to the lack of a suitable single-phase test case modeled by barotropic flow system (2.1) and with smooth exact solution, a one-dimensional (1D) Riemann problem involving discontinuity is resolved to check order of accuracy of our method. Initially, two water streams are moving in the opposite direction away from the center of $1m$ long tube at the velocity magnitude of $50m/s$. The pressure is 10^8Pa throughout the domain. Two-dimensional (2D) unstructured mesh is used with y velocity component set to 0 at the initial time.

The simulation is run to $t = 0.2ms$. The solution is composed of a left rarefaction, a right rarefaction and a stationary contact discontinuity in between. In this case, cavitation does not occur as velocity magnitude is not high enough. Four sets of triangular mesh are used with characteristic grid length of $\Delta h_k = 1/N_k$ where $N_k = 160, 320, 640$ and 1280 . Fig. 3 plots L_1 error norm in the density and x velocity against h_k . The L_1 error norm is defined as $L_1 = \sum_{i=1}^{N_m} |w_i - w_{exact}| \Delta \Omega_i$, where w_i is the numerical solution of density or x velocity in cell i , w_{exact} is the corresponding exact solution, $\Delta \Omega_i$ is area of cell i and N_m is the total number of mesh elements. As shown in Fig. 3, MUSCL is only first-order accurate for this case. This is due to the fact that the scheme with limiter locally degrades to first-order accuracy in the presence of large gradients. The method should still be second order accurate in smooth part of the solution.

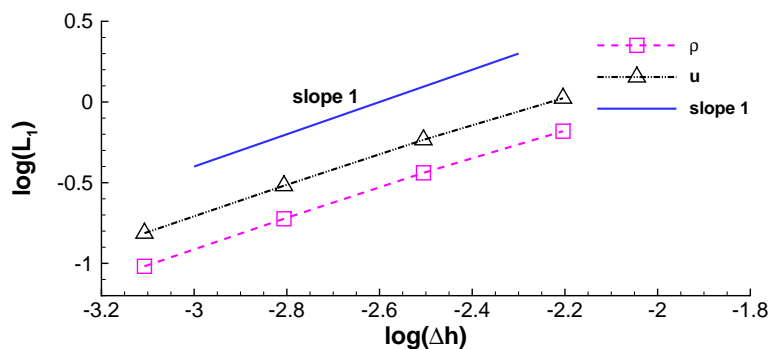


Figure 3: L_1 error norm in the density and x velocity component for the 1D Riemann problem.

3.2. One-dimensional shock tube problem

Next, a 1D Riemann problem is simulated. Initially, the left side of $1m$ long shock tube is filled with liquid water with density of $1200kg/m^3$ whereas the right side is filled with water-vapour mixture with density of $500kg/m^3$. As the mixture density is smaller than the saturated density, the right region is cavitation region. The fluid is at rest throughout the domain. Calculation is carried out on a 2D mesh with $\Delta h = 1/2000m$.

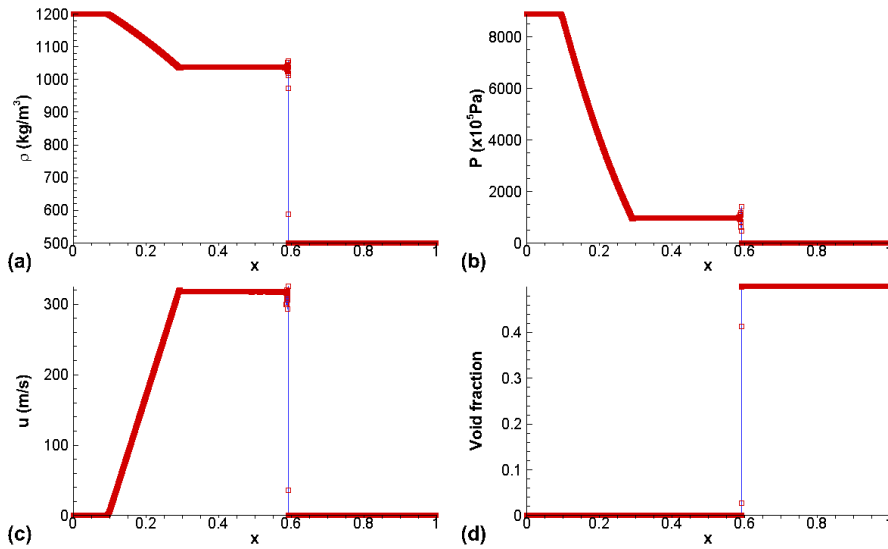


Figure 4: The numerical solution to the 1D shock tube problem at time $t = 150\mu s$.

The solution of this problem consists of a leftward-going rarefaction in liquid water and a rightward-going shock. The numerical solution at time $t = 150\mu s$ is presented in Fig. 4. Both the shock wave and rarefaction wave are well resolved as illustrated in Fig. 4. The shock propagation through cavitation causes high pressure increase. As a result, the vapour condenses instantaneously with void fraction dropping from around 0.5 to 0, see Fig. 4. Our results are comparable to those of [2].

3.3. Two-dimensional supersonic cavitating flow

The third case is a further more complex verification of our code. This is on the resolution of the two-dimensional axisymmetric supercavitation around an object which is impulsively started in pure water flow at the steady inflow velocity of 3000m/s corresponding to a Mach number of approximately 2 and at standard pressure. The underwater body consists of three parts: a nose cone with half-angle of 45° and base radius of 1cm, a cylinder of length 1cm and a rear cone with semi-vertex angle of 45° . The computational domain is 0.43m long and 0.4m high. The flow is symmetric about the line of symmetry of the object because the angle of attack is 0. Therefore, only the upper half of the flow field is resolved. The left and right sides of the computational domain are treated as inflow and non-reflecting boundaries, respectively, whereas the symmetry axis and body surface are considered as reflecting boundaries. The simulation setup is similar to those in [2, 3] to facilitate the comparison of numerical results. An unstructured mesh of 229,554 triangular elements are used.

This is a supersonic flow around blunt object and thus a detached bow shock is expected to appear in front of the cone and the body is to be enveloped by the super-

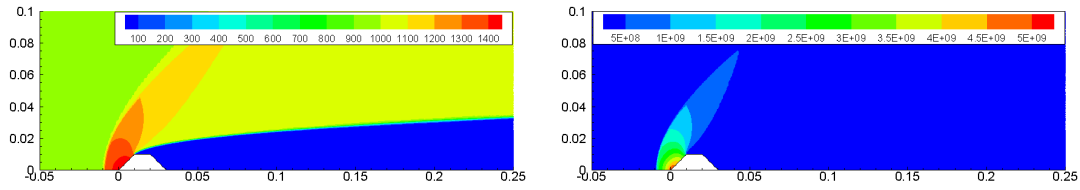


Figure 5: Two-dimensional steady supersonic cavitating flow: (a) density contour; (b) pressure contour.

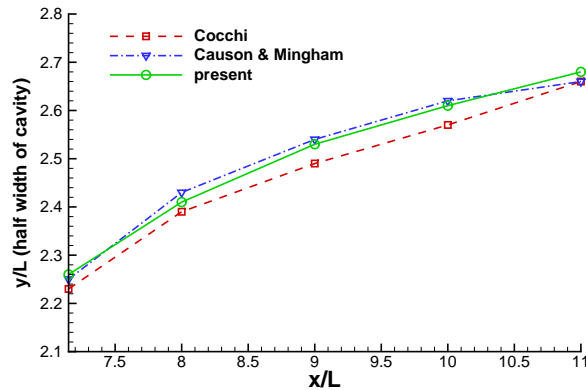


Figure 6: Comparison of calculated cavity half widths from Cocchi [3], Causon and Mingham [2] and the present study.

cavitation bubble. These flow features are well captured as illustrated in the density and pressure contour images at the steady state shown in Fig. 5 where the large density and pressure jumps across the shock and cavitation boundary are observed. The detached shock shape and standoff distance are qualitatively consistent with those reported in [2,3]. The cavitation, indicated in blue in the density contour of Fig. 5, starts on the transition region between cone and cylinder and extends downstream, forming a cavitation pocket covering the entire object except for the nose. Quantitatively, the predicted steady state cavity half widths from Cocchi [3], Causon and Mingham [2] and the present study are compared in Fig. 6 where the values are normalized by the cylinder length $L = 1\text{cm}$. It is obvious that our results are in a satisfactory agreement with [2,3]. It is unfortunate that there is a lack of experimental data for further comparison.

As mentioned earlier, we are concerned with the unsteady dynamics of supercavitation disturbed by external perturbations. Here, the initial condition for the unsteady calculation is based on the converged steady solution obtained in the simulation mentioned above. Next, the region to the left of $x = -0.05\text{m}$ is initialized with the post-shock state corresponding to a specific shock Mach number. After $70\mu\text{s}$, the inflow condition returns to its original values specified in the previous steady state simulation. The time evolution of density field with $\text{Ma}=3.1$ is presented in Fig. 7. The time indicated in Fig. 7 is measured from the instant when the shock is introduced. It is

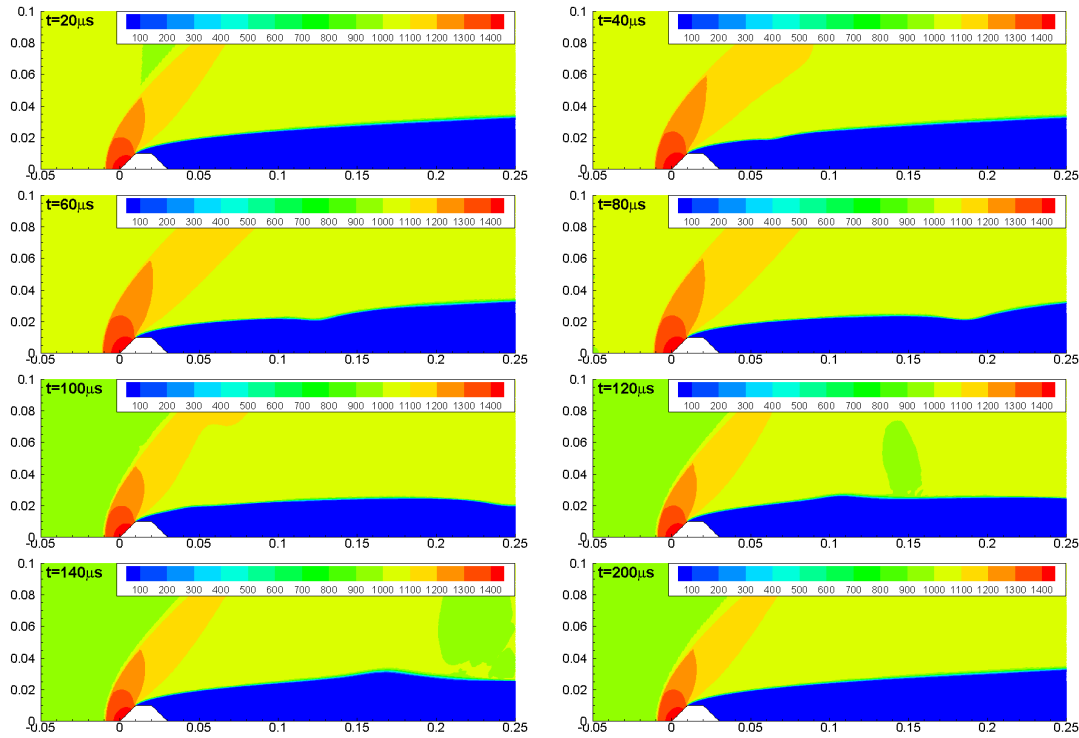


Figure 7: The time evolution of cavitation impacted by a Mach 3.1 shock wave.

observed that the cavity boundary locally experiences small deformation but quickly recovers to its original profile. This process lasts for a duration of around $200\mu s$. The shock wave leads to a high pressure increase of order of $\mathcal{O}(10^8)$ Pa across its front. The fact that the cavity is not induced to collapse by the strong impact indicates that the cavitation is relatively stable at high freestream velocity. The situation associated with a higher shock Mach number $Ma=3.2$ is shown in Fig. 8. The difference between two cases is that the cavity undergoes a more severe deformation and locally collapses at the higher Mach number. To quantify the response of the body to perturbation, the time history of unsteady drag coefficient is recorded and plotted in Fig. 9. The value of form drag coefficient is increased significantly in a short period of time during which the shock-cavitation interaction takes place. The increase for $Ma=3.2$ is about two times that with $Ma=3.1$.

3.4. Unsteady cavitation around a blunt head cylinder

The fourth case is the calculation of interaction between cavitation around a blunt-head cylinder and pressure wave. The freestream velocity is $U_\infty = 200m/s$ and parallel to the cylinder, which means that this is a low subsonic flow. The computational domain has the length of $0.5m$ and height of $0.4m$. To save computational cost, simulation is

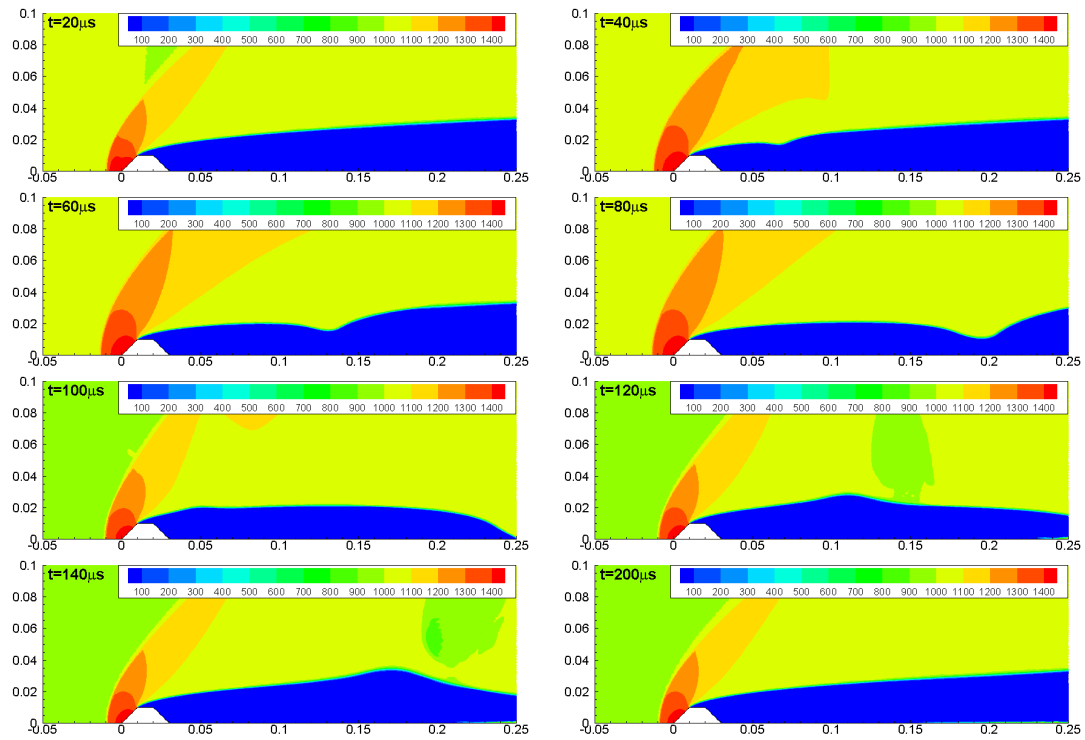


Figure 8: The time evolution of cavitation impacted by a Mach 3.2 shock wave.

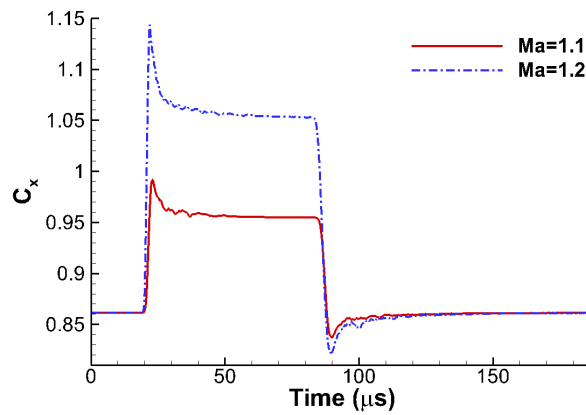


Figure 9: The time history of drag coefficient for the body in Figs. 7 and 8.

carried out on the upper half of the domain. The mesh used consists of around 96,000 cells. The initial condition for the unsteady calculation is the converged solution at $U_\infty = 200\text{m/s}$ except that a high pressure p_h is specified in the region to the left of $x = -0.2\text{m}$ to generate a pressure wave. The density field evolution processes associated with $p_h = 2 \times 10^7\text{Pa}$, $4 \times 10^7\text{Pa}$ are presented in Fig. 10 for comparison.

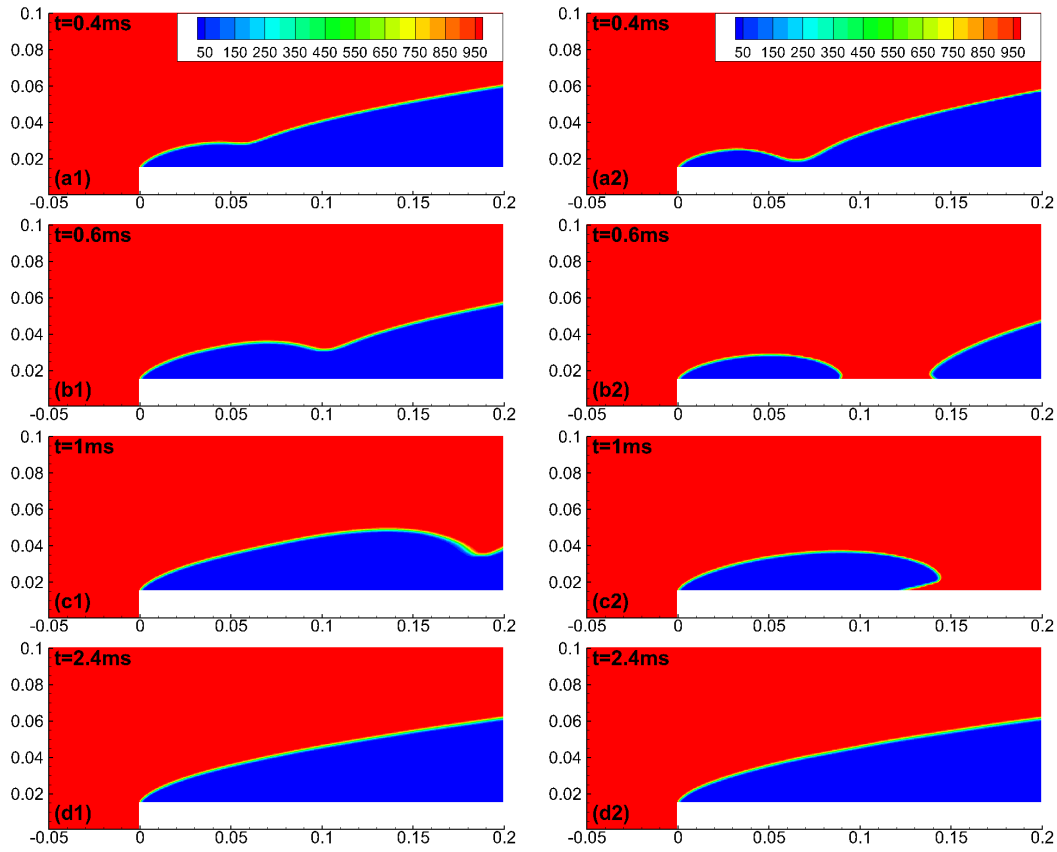


Figure 10: The unsteady cavitation around a cylinder. First column: $P_h = 2 \times 10^7\text{Pa}$; second column: $P_h = 4 \times 10^7\text{Pa}$.

In Fig. 10, $t = 0$ corresponds to the start time of unsteady calculation. The pressure wave generated by $p_h = 2 \times 10^7\text{Pa}$ is relatively weak and cavity is distorted by the wave only and the deformed cavitation interface recovers to the smooth profile fairly quickly; see the first column of Fig. 10. However, when P_h is increased to $4 \times 10^7\text{Pa}$, the cavity locally collapses and is divided into two parts, as shown in the second column of Fig. 10. Eventually, the left partial cavity develops into a supercavity. Obviously, the lower magnitude pressure wave upstream has less devastating effect on the original supercavity. Our study shows the critical importance of upstream perturbation which can lead to the collapse of the original steady state supercavity with induced large form drag and potential destabilization of the moving submerged body.

4. Conclusion

The unsteady cavitating flow due to the pressure wave impact has been numerically simulated using a CFD code based on the homogeneous one-fluid cavitation model. The

cavity deformation and collapse caused by the pressure wave are affected by the pressure wave strength and magnitude of freestream velocity. The drag acting on the body is increased significantly during a short time period. The main unsteady features of the interaction between pressure wave and cavitation have been successfully resolved.

Acknowledgments The work is supported by ONR (Office of Naval Research) under grant number N000141010474.

References

- [1] J. BLAZEK, *Computational fluid dynamics: principles and applications*, ELSEVIER, 2001.
- [2] D. M. CAUSON AND C. G. MINGHAM, *Finite volume simulation of unsteady shock-cavitation in compressible water*, *Int. J. Numer. Meth. Fluids*, 72 (2013), pp. 632–649.
- [3] J. P. COCCHI, *Quelques contributions aux traitements numeriques de problemes a interface liquide-vapeur. Application a la cavitation aux hypervitesses*, PhD Thesis, Universite de Provence (Aix-Marseille I), (1997).
- [4] Z. M. HU, H. S. DOU AND B. C. KHOO, *On the modified dispersion-controlled dissipative (DCD) scheme for computation of flow supercavitation*, *Comput. Fluids*, 40 (2011), pp. 315–323.
- [5] R. F. KUNZ, D. A. BOGER AND D. R. STINEBRING, *A preconditioned Navier-Stokes method for two-phase flows with application to cavitation prediction*, *Comput. Fluids*, 29 (2000), pp. 849–875.
- [6] T. G. LIU, B. C. KHOO AND W. F. XIE, *Isentropic one-fluid modeling of unsteady cavitating flow*, *J. Comput. Phys.*, 201 (2004), pp. 80–108.
- [7] M. D. NEAVES AND J. R. EDWARDS, *All-speed time-accurate underwater projectile calculations using a preconditioning algorithm*, *J. Fluids Eng.*, 128 (2006), pp. 284–296.
- [8] R. SAUREL, F. PETITPAS AND R. A. BERRY, *Simple and efficient relaxation methods for interfaces separating compressible fluids, cavitating flows and shocks in multiphase mixtures*, *J. Comput. Phys.*, (228) 2009, pp. 1678–1712.
- [9] D. P. SCHMIDT, C. J. RUTLAND AND M. L. CORRADINI, *A fully compressible two-dimensional model of small high speed cavitating nozzles*, *Atomization Sprays*, 9 (1999), pp. 255–276.
- [10] S. J. SCHMIDT, I. H. SEZAL, G. H. SCHNERR AND M. TALHAMER, *Riemann techniques for the simulation of compressible liquid flows with phase-transition at all Mach numbers - shock and wave dynamics in cavitating 3-D micro and macro systems*, AIAA paper, (2008) pp. 092407(1–24).
- [11] S. J. SCHMIDT, M. TALHAMER AND G. H. SCHNERR, *Inertia controlled instability and small scale structures of sheet and cloud cavitation*, *Proceedings of the 7th International Symposium on Cavitation*, (2009) pp. 17(1–14).
- [12] C. W. SHU AND S. OSHER, *Efficient implementation of essentially non-oscillatory shock capturing schemes*, *J. Comput. Phys.*, 77 (1988), pp. 439–471.
- [13] M. Y. SUN AND T. KOITA, *Numerical and experimental study of secondary cavitation induced by underwater electric discharge in a tube*, doi:10.3850/978 – 981 – 07 – 2826 – 7_241.
- [14] M. Y. SUN, *A thermodynamic and dynamic subgrid closure model for two-material cells*, *Int. J. Numer. Meth. Fluids*, 73(2) (2013), pp. 130–151.
- [15] E. F. TORO, *Riemann solvers and numerical methods for fluid Dynamics: a practical introduction*, Springer-Verlag, Berlin Heidelberg, 1999.

- [16] B. VAN LEER, *Towards the ultimate conservative difference scheme V. A second-order sequel to Godunov's method*, J. Comput. Phys., 32 (1979), pp. 101–136.
- [17] B. VAN LEER, *Upwind and High-Resolution Methods for Compressible Flow: From Donor Cell to Residual-Distribution Schemes*, Commun. Comput. Phys., 1(2) (2006), pp. 192–206.
- [18] G. B. WALLIS, *One-dimensional two-phase flow*, New York: McGraw-Hill, 1969.
- [19] L. X. ZHANG AND B. C. KHOO, *Computations of partial and super cavitating flows using implicit pressure-based algorithm (IPA)*, Comput. Fluids, 73 (2013), pp. 1–9.
- [20] J. G. ZHENG, B. C. KHOO AND Z. M. HU, *Simulation of wave-flow-cavitation interaction using a compressible homogenous flow method*, Commun. Comput. Phys., 14(2) (2012), pp. 328–354.